Bulk metallic glass formation in the Mg–Cu–Y system

A. Katz-Demyanetz[1], H. Rosenson[1], Z. Koren[1] and M. Regev[2]*

The influence of the cooling rate on 80Mg–15Cu–5Y was investigated. Four different cooling rates yielded different microstructures that were characterised by means of X-ray diffraction (XRD), SEM, high-resolution SEM, energy dispersive spectroscopy chemical analysis, TEM and high-resolution TEM. The different casting procedures were gravity castings of 3 mm diameter specimens into a copper mould held at different temperatures (cooled to −195°C with the aid of liquid nitrogen, held at room temperature and heated to 300°C) and melt spinning. Only the melt spun specimen yielded what appeared to be an amorphous XRD spectrum; however, a detailed TEM analysis showed that this specimen was characterised by a micro- or even nanocrystalline rather than amorphous structure.

Keywords: Microstructure, Gravity casting, Permanent mould casting, Melt spinning, Metallic glass

Published by Maney Publishing (c) IOM Communications Ltd

Introduction

Magnesium alloys are attractive for engineering applications such as the automotive industry owing to their good physical properties; namely, high strength, light weight, good damping absorption and good thermal and electrical conductivity. Furthermore, amorphous magnesium alloys exhibit higher strength, hardness and a large elastic domain in addition to excellent corrosion resistance.[1–6] Until the 1980s very high cooling rates were required in order to avoid crystallisation, leading to the availability of metallic glasses only as thin foils, i.e. splats or ribbons. Today, the necessary chemical compositions are known, so that bulk metallic glasses (BMGs) can be produced.[3] Among the various existing magnesium alloys, the Mg–Cu–Y system is known as one of the best glass formers.[5]

The growing interest in high glass-forming abilities (GFAs) has led to the formulation of semiempirical rules for producing BMGs: (1) multicomponent systems (the confusion principle); (2) a significant difference in atomic size, above 12% between the main constituent elements; (3) the occurrence of large negative enthalpy of mixing; and (4) compositions close to deep eutectics.[4,7]

Below is a summary of the research work dealing with the microstructure of amorphous Mg–Cu–Y alloys reported in the literature.

Hong *et al.*[1] prepared 60Mg–30Cu–10Y powders by the droplet emulsion technique (DET). They achieved undercooling of 60–140 K by controlling the powder size. The microstructure obtained changed with the degree of undercooling from lamellar eutectic to dendritic, to cellular and, finally, to a glassy phase.

Pryds *et al.*[5] obtained amorphous 60Mg–30Cu–10Y by quenching the melt into a plate-shape copper mould. They studied the crystallisation kinetics of the amorphous alloy by means of differential scanning calorimetry (DSC) but no microstructure characterisation was reported.

Savyak *et al.*[6] prepared 65Mg–25Cu–10Y glassy ribbons by melt spinning. A TEM study performed by them revealed an amorphous matrix phase with a few embedded nanocrystals 5–15 nm in size.

Satta *et al.*[7] investigated two different compositions, 27Mg–38Cu–35Y and 65Mg–25Cu–10Y, prepared by a melt spinning technique. They found that the 27Mg–38Cu–35Y composition, which remained far from the glass-forming range, did not show amorphisation under rapid solidification whereas full amorphisation was obtained in the case of 65Mg–25Cu–10Y.

Inoue *et al.*[8,9] pointed out the maximum diameters for the formation of an amorphous single phase for 90–*x*Mg–*x*Cu–10Y produced by high-pressure die casting. They found that the maximum diameter varies from 3 mm for a Cu content of 10at.-% up to 7 mm for a Cu content of 25at.-%. After performing tension tests on an amorphous 80Mg–10Cu–10Y high-pressure die cast specimen, they found that the fracture stress at room temperature (RT) is 630 MPa without appreciable elongation. A DSC study of 65Mg–25Cu–10Y showed that there was no appreciable difference in the glass transition temperature (T_g) and the onset temperature of crystallisation (T_x) values between the cast and melt spun samples.[9] In another study Inoue *et al.*[10] compared T_g and T_x values of an Mg–Cu–Y metallic mould casting with those of a 0·02 mm thickness melt spun ribbon and came to the same conclusion; namely, they saw that there was no appreciable difference in the values of T_g and T_x between the two processes. The critical diameter

[1]Israel Institute of Metals, Foundry Laboratory, Technion–Israel Institute of Technology
[2]Ort Braude College of Engineering, Mechanical Engineering Department, P.O.B. 78, Karmiel, Israel

*Corresponding author, email michaelr@braude.ac.il

© 2009 Institute of Materials, Minerals and Mining
Published by Maney on behalf of the Institute
Received 8 May 2008; accepted 6 August 2008
DOI 10.1179/174328408X374658

for the formation of an amorphous phase in the case of metallic mould casting was in the range 1·0–4·0 mm in the composition range 10–35%Cu and 10–20%Y and reached the maximum value for 65Mg–25Cu–10Y.

Wolff *et al.*[11] prepared bulk amorphous 60Mg–30Cu–10Y alloys by rapid quenching in a copper mould. They found that controlled annealing of these specimens at 174°C for different periods led to various degrees of partial crystallisation, namely 15%, 50%, 75% and 100%. X-ray diffraction (XRD) and TEM studies of the microstructure obtained revealed only a crystalline 2Mg–Cu orthorhombic phase. No equilibrium Mg–Y phase such as 24Mg–5Y or 2Mg–Y was detected. The average grain size of the crystalline phase was about 100 nm; the nanocrystallised specimens showed an increase in the yield stress provided that their crystalline volume fraction was less than 50%. Larger volume fractions of nanocrystals promoted brittle fracture and reduced strength.

Chen and Ferry[12] studied the crystallisation behaviour of 65Mg–25Cu–10Y bulk metallic glass produced by mould casting by exposing it to 210°C, 230°C and 250°C for 3, 6 and 9 minutes, respectively. They used XRD, DSC and SEM for their investigation and found that the fully amorphous phase transforms into an amorphous phase containing 2Mg–Cu and, finally, into a Mg solid solution containing 2Mg–Cu, 24Mg–5Y and 2Cu–Y.

Kim *et al.*[13] used XRD and TEM for studying the compositional range in which an amorphous phase in the Mg–Cu–Y system is formed by melt spinning. They claimed that both compositions, 80Mg–10Cu–10Y and 80Mg–15Cu–5Y, yield an amorphous phase under rapid cooling rates. The value they found for ΔT_x ($=T_g-T_x$) was about 20 K for both compositions.

Murty and Hono[14] studied the microstructure of melt spun 65Mg–25Cu–10Y, 80Mg–10Cu–10Y and 80Mg–15Cu–5Y by means of TEM, XRD and DSC. They concluded that nanodispersions of 2Mg–Cu, hcp-Mg and fcc-Mg with particle sizes of 5–20 nm were observed within the amorphous matrix of the 65Mg–25Cu–10Y, 80Mg–10Cu–10Y and 80Mg–15Cu–5Y alloys, respectively.

Ma *et al.*[15] showed, by means of DSC and XRD, that the optimal Mg–Cu–Y bulk metal glass formers are close to, but do not quite match, the eutectic composition. They showed that relatively small composition differences can result in doubling of the critical size for bulk metallic glass formation compared with the critical size for eutectic composition.

The current paper deals with the alloy 80Mg–15Cu–5Y. To the best of the authors' knowledge, a study about the influence of the cooling rate on the microstructure together with a detailed microstructure characterisation for this composition is still lacking.

Most investigators have studied compositions of relatively low Mg content (less than 65at.-%). In such cases obtaining high GFA is mainly due to the presence of elements with significantly different atomic radii (rules 1 and 2 mentioned above). The alloy 80Mg–15Cu–5Y was chosen for two main reasons: (1) its low density (less than the density of Al-based alloys) and (2) the fact that the Mg/Cu ratio is close to Mg–Cu eutectic. One can see that the first reason is related to possible applications of the alloy while the second one originates from high GFA (see rule 4 mentioned above). Keeping in mind that the Y atomic radius of 2·27 Å is markedly different from that of Mg (1·72 Å) and Cu (1·57 Å) – these differences are significantly higher than the difference between Mg and Cu atomic radii – and that the Y content is relatively low, it was assumed that Y would dissolve in the Mg–Cu matrix rather than help create an intermetallic phase. The rationale behind this assumption is that the low Y concentration dictates a relatively large diffusion path while the differences in the atomic radii retard Y diffusion within the Mg–Cu matrix. Suppression of possible Y segregation by rapid solidification may, in turn, lead to high GFA and thus to amorphous structure formation. It was supposed that cooling rates slower than those required to suppress Y-rich phase formation would lead to crystallisation. The current study checks this approach. The casting processes chosen for this study were different gravity casting and melt spinning processes because of their industrial applicability.

Experimental

The chemical composition 80Mg–15Cu–5Y was selected for the current study owing to its proximity to the eutectic composition, and hence the synthesised material could be expected to have an improved GFA. Pure Mg and Cu metals and Mg–40Y (wt-%) master alloy were used for the alloy preparation. Alloying was performed in a graphite crucible under an Ar protective atmosphere. The materials blend was melted and then homogenised at 750°C for 1 hour before casting. The alloy was then gravity-cast into a steel mould and air cooled to RT.

Gravity casting of 3 mm diameter specimens into a copper mould held at different temperatures (cooled to −195°C with the aid of liquid nitrogen, held at room temperature and heated to 300°C) and melt spinning were used in order to test various cooling rates. The details of the casting experiments are listed in Table 1. In all cases of gravity casting the temperature of the melt was measured by using a K type thermocouple; hence, cooling rates could be calculated. For process 1, the cooling rate was found to be around 1°C s^{-1}, in the case of the mould held at RT the cooling rate was found to be about 10°C s^{-1} and in the case of the mould held at −195°C the cooling rate was found to be about 100°C s^{-1}. As for the melt spinning process, the cooling rate was estimated to be about 1 000 000°C s^{-1}. This estimation

Table 1 Casting experiments

No.	Casting process	Details
1	Permanent Cu-mould	Mould held at 300°C
2	Permanent Cu-mould	Mould held at RT
3	Permanent Cu-mould	Mould held at −195°C
4	Melt spinning	Wheel rotation − 1000 rpm, Ar atmosphere

Published by Maney Publishing (c) IOM Communications Ltd

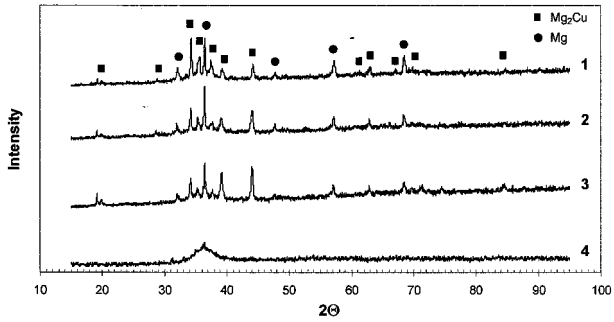

1 XRD patterns of 80Mg–15Cu–5Y under various casting conditions and processes

is based on both literature[16] and a heat transfer calculation taking the thickness of the specimen and the geometry of the machine into account.

X-ray diffraction tests were performed by using a Philips PW-1820 Bragg–Brentano geometry equipped with a Cu tube ($\lambda_{K\alpha}$=1·5406Å). The melt spun specimen was ground to powder prior to the XRD tests in order to eliminate any texture influence. The microstructure was studied under a 20 kV Philips XL30 SEM equipped with an Oxford EDS system and with a 5 kV Leo-982 high-resolution SEM (HRSEM). Investigation by TEM was conducted by using an FEI Tecnai T20 200 kV TEM and an FEI Titan 300 kV high-resolution TEM.

TEM specimens were prepared as follows:

1. 80 μm thick slices were cut from the melt spun film
2. the slices were ion milled using a Gatan-600 laser-terminated dual ion miller with an acceleration voltage of 5 kV and a current of 5 mA. The initial milling angle was 25°, which was then changed to 10°. The specimens were continually cooled with the aid of liquid nitrogen in order to avoid artefacts resulting from specimen heating.

Results

X-ray diffraction spectra of specimens cast by the four processes listed in Table 1 are given in Fig. 1. The numbering of the casting processes is identical to the numbering in Table 1. The phases identified are Mg and 2Mg–Cu; their peaks are shown in Fig. 1. Some peaks remained unidentified. It can be seen from Fig. 1 that the only spectrum having an amorphous pattern is spectrum 5; namely, the specimen cast by the melt spinning process.

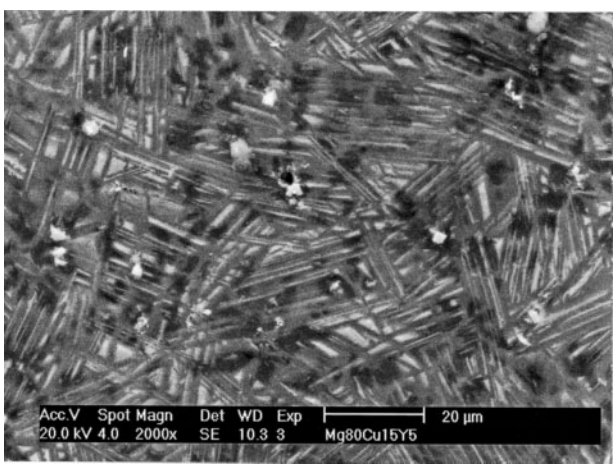

2 SEM micrograph of the gravity casting, mould held at 300°C

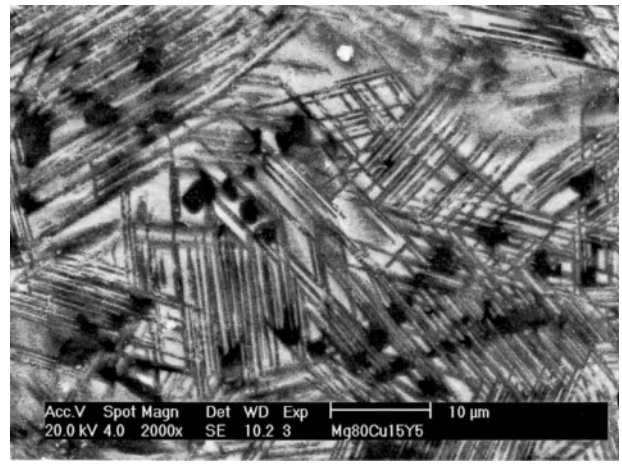

3 SEM micrograph of the gravity casting, mould held at RT

An SEM micrograph of the permanent Cu mould, held at 300°C, casting given (Fig. 2) is characterised by an acicular morphology. Dark regions are discernible within the acicular structure even though they are not so clearly detected. Shiny bright particles having an average size of about 1 μm are scattered all over the specimen. Analysis by EDS showed that the bright particles contain a high concentration of Y, about 60at.-%. The chemical composition of the acicular structure is close to 80at.-%Mg and 20at.-%Cu; it contains about 5%Y. The dark regions are Mg with about 4at.-%Cu and 3at.-%Y.

An SEM micrograph of the permanent Cu mould, held at RT, casting is shown in Fig. 3. A few phases can be detected in this micrograph; namely, a dark one, an acicular one and bright particles. Analysis by EDS showed that the chemical composition of the acicular phase is close to 80at.-%Mg and 20at.-%Cu containing about 5at.-%Y while the dark one is Mg with about 4at.-%Cu and about 1at.-%Y. The bright particles contain a high concentration of Y, as in Fig. 2.

An SEM micrograph of the permanent Cu mould, held at −195°C, casting is shown in Fig. 4. The microstructure is composed of a fine acicular structure containing dark particles. A high-resolution SEM image of one of these dark particles with the acicular structure next to it is presented in Fig. 5. It can be seen that the

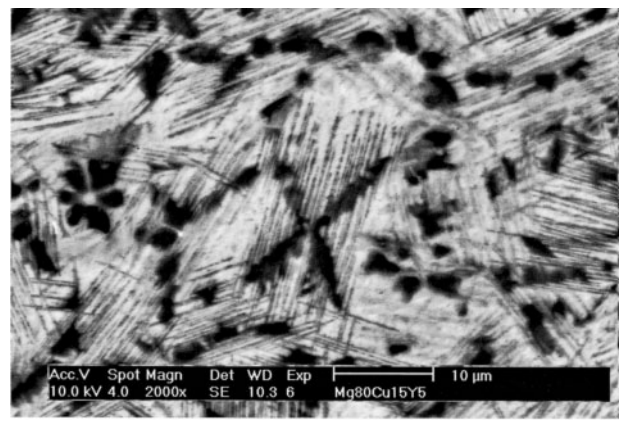

4 SEM micrograph of the gravity casting, mould held at −195°C

Published by Maney Publishing (c) IOM Communications Ltd

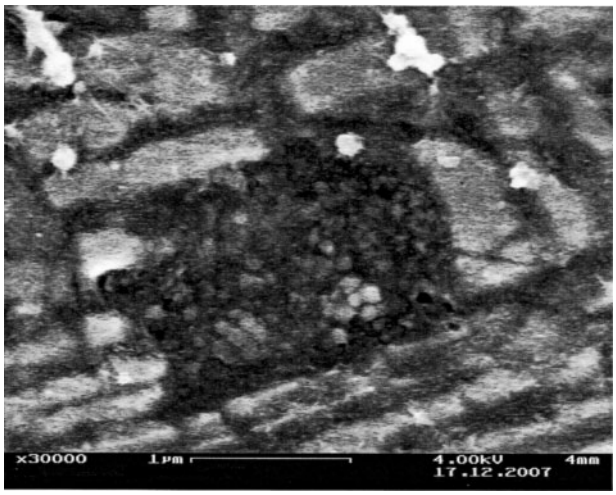

5 HRSEM micrograph of the gravity casting, mould held at −195°C

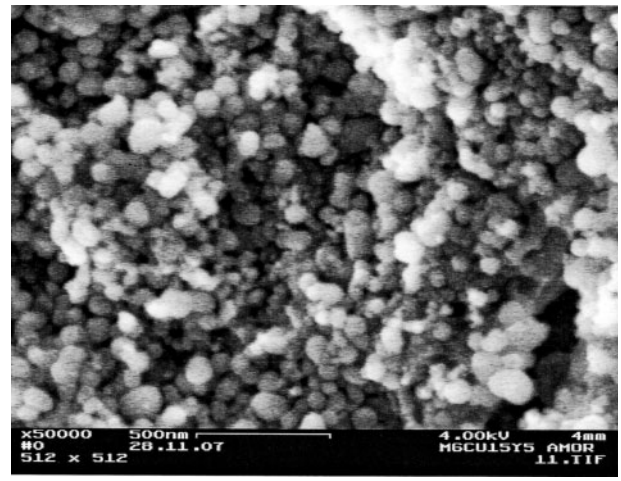

6 HRSEM micrographs of the specimen cast by melt spinning

dark particle is composed of nanospherical particles and that the thickness of the aciculas is about 10 nm. Analysis by EDS showed that the chemical composition of the acicular phase is close to 80at.-%Mg and 20at.-%Cu, the dark phase is Mg with about 9at.-%Cu and about 2at.-%Y, and the bright particles are characterised, as in all other cases, by a Y concentration of more than 50at.-%.

A HRSEM micrograph of the specimen cast by the melt spinning process is shown in Fig. 6. It can be seen that the microstructure consists of nanospheres. The size of these spheres is a few tens of nanometres each.

A TEM bright-field image and the respective selected area diffraction pattern are shown in Fig. 7, whereas Fig. 8 presents HRTEM images. It can be seen from Fig. 7 that the specimen contains nanograins. A good estimation of their size can be obtained when looking at the dark grains, those that are tilted into zone axes. They are the same size as those detected by the HRSEM. The ring diffraction pattern is typical for nanograined material.

The high-resolution image appearing in Fig. 8 clearly shows a nanocrystalline structure. A few grains are discernible and their size is in line with the previous findings of the HRSEM and TEM examinations. The different lattice orientation of adjacent grains is discernible. The respective Fast Fourier Transform (FFT) performed on part of the grains shown in Fig. 8 are given as well. The different FFT patterns clearly prove that these nanograins are crystalline and that their orientations are different.

Discussion

The XRD patterns observable in Fig. 1 show evidence of amorphous structure only in the case of the melt spun specimen. In the rest of the casting processes used in this study, Mg and 2Mg–Cu peaks were identified in all cases. No reflections of free Y were detected in the crystalline alloys examined, possibly because of its small volume fraction. However, Mg and 2Mg–Cu reflections are slightly shifted to lower angles (higher d-spacings),

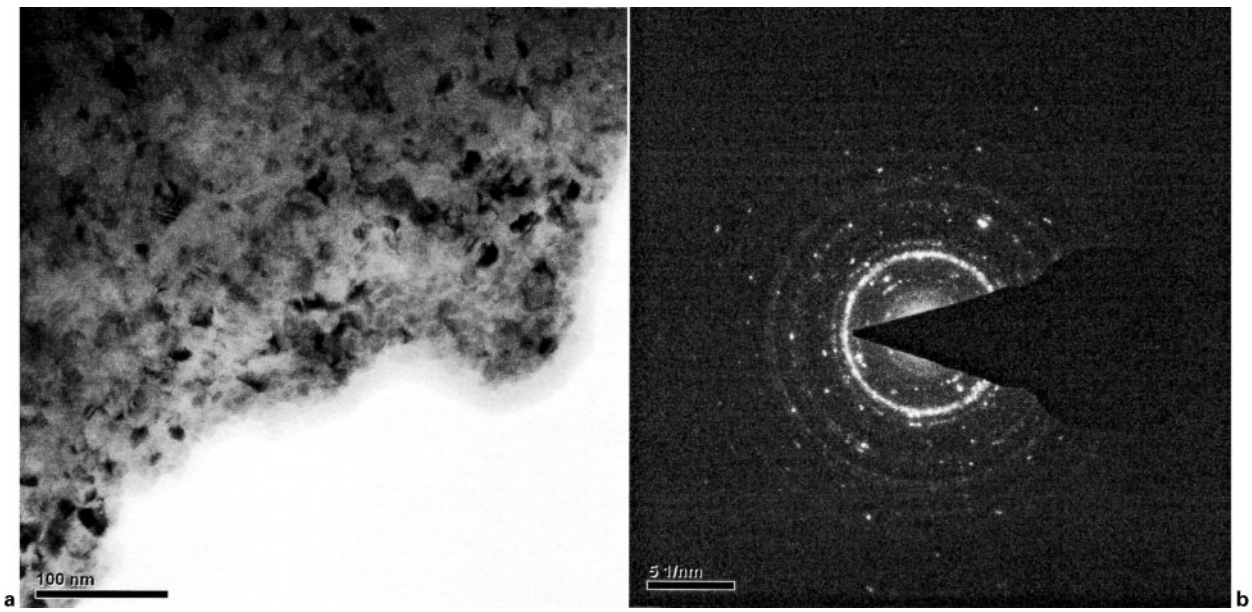

a bright field image; *b* selected area diffraction pattern

7 TEM micrographs of the specimen cast by melt spinning

Published by Maney Publishing (c) IOM Communications Ltd

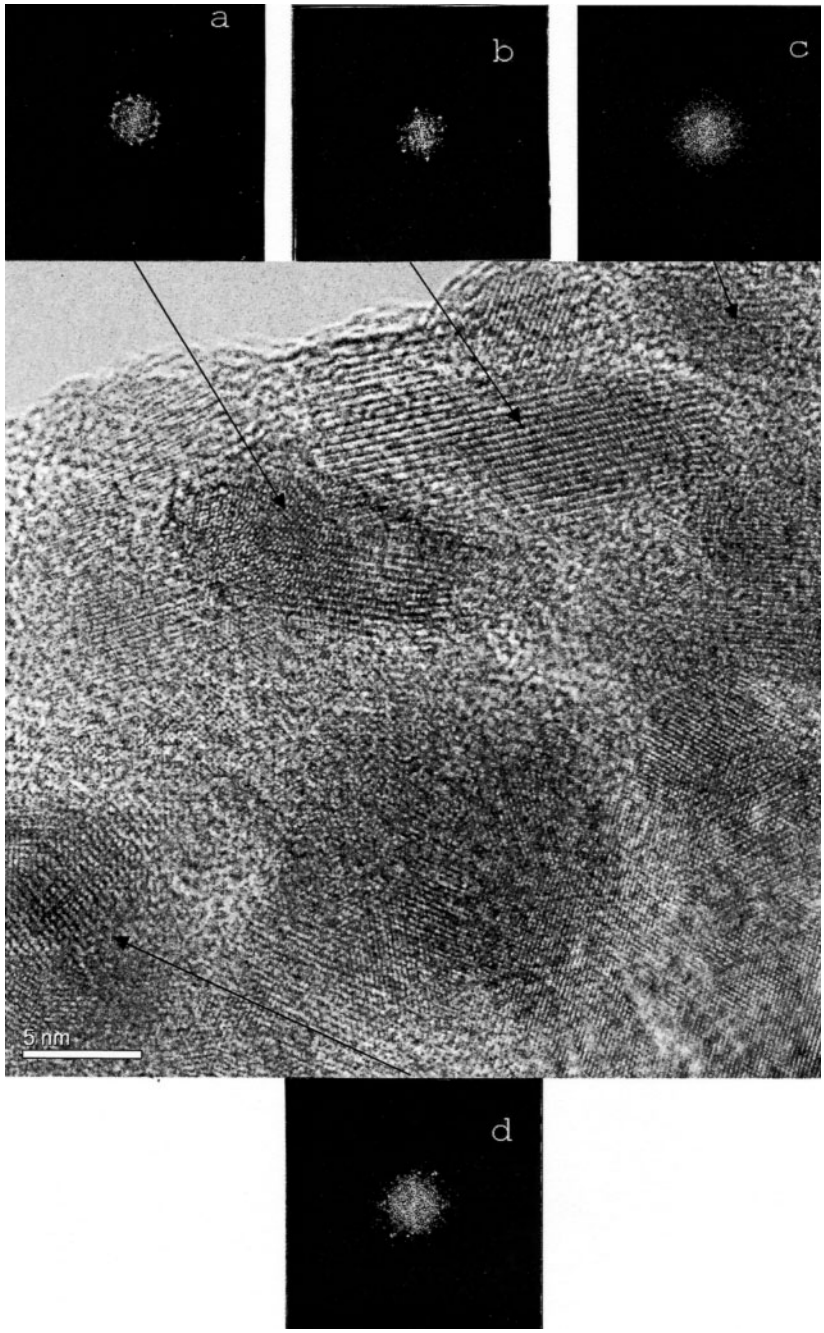

8 HRTEM micrograph of the specimen cast by melt spinning with the respective FFTs

possibly due to the existence of dissolved Y. Mg–Cu and Mg–Y phase diagrams are shown in Figs. 9 and 10, respectively. It can be seen that with a Cu content of 10at.-% both Mg and 2Mg–Cu are expected to coexist at RT under equilibrium conditions. As for the Mg–Y phase diagram, the maximum Y content does not exceed 1·5at.-% at 400°C and the maximum solubility limit is even lower at RT. The Y is, therefore, expected to appear in a Mg solid solution and in either 24Mg–5Y or 5Mg–2Y intermetallics.

A SEM study revealed an acicular structure in the case of the gravity casting when the Cu mould was held at 300°C (Fig. 2). The chemical composition of this acicular structure was found to be close to 80at.-%Mg and 20at.-%Cu. However, the existence of a phase having such a composition is not expected according to the respective phase diagram and was not detected by XRD as stated earlier. It may be concluded, therefore, that this composition was recorded owing to limitations of the EDS system; namely, the relatively large excited volume that led to obtaining the 80at.-%Mg and 20at.-%Cu stoichiometric relation due to some averaging between the existing phases, specifically Mg and 2Mg–Cu. The dark regions in Fig. 2 being Mg with about 4at.-%Cu and 3at.-%Y is in line with the Mg–Cu phase diagram (Fig. 10) and with the XRD spectrum (Fig. 1). The Y concentrations within the bright phase seen in Fig. 2 are far from the Y concentrations in the 24Mg–5Y or 5Mg–2Y intermetallics and it may be concluded, therefore, that these bright particles are non-dissolved Y. The high concentrations of dissolved Y and Cu can be related to the non-equilibrium cooling conditions, which thus yielded a supersaturated solid solution. The same analysis can be applied to the other two gravity casting processes; namely, when the mould temperature was the RT and −195°C (Figs. 3 and 4, respectively).

Published by Maney Publishing (c) IOM Communications Ltd

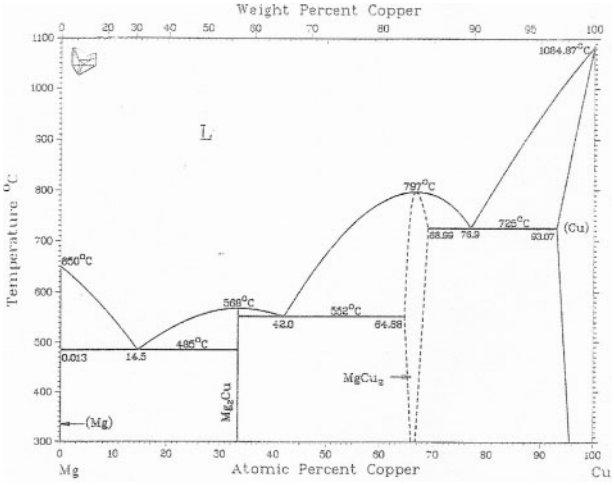

9 Mg–Cu phase diagram[17]

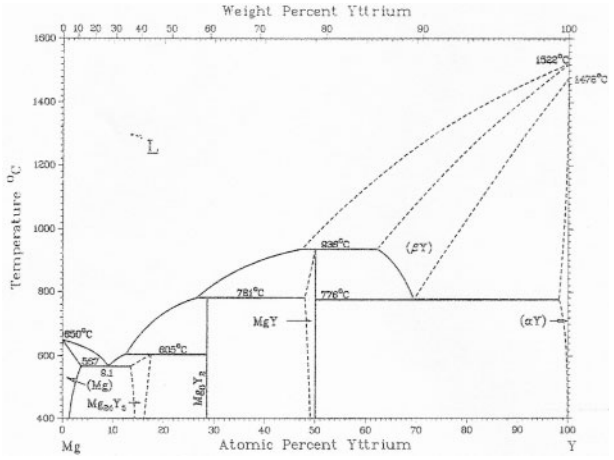

10 Mg–Y phase diagram[17]

In the case of gravity casting while keeping the mould at room temperature (Fig. 3), the microstructure is similar to that of Fig. 2. The only difference observed is the degree of fineness of the acicular structure, which seems to be finer than the one obtained when the mould was held at 300°C (Fig. 2). The same explanation for the chemical composition of the acicular phase being close to 80at.-%Mg and 20at.-%Cu can, in the authors' opinion, be adopted. The dark regions in Fig. 3 being Mg with about 4at.-%Cu and 1at.-%Y is in line, once again, with the Mg–Cu phase diagram (Fig. 10) and with the XRD spectrum (Fig. 1). The Y concentrations within the bright phase are again markedly higher than those expected in the case of 24Mg–5Y or 5Mg–2Y intermetallics. It may be concluded, therefore, that these bright particles are non-dissolved Y. The high concentrations of dissolved Y and Cu can be related to the non-equilibrium cooling conditions, which thus yielded a supersaturated solid solution. As for the third gravity casting process, namely gravity casting while keeping the mould temperature at −195°C, the acicular phase is even finer, as evident in Fig. 5. The 80at.-%Mg and 20at.-%Cu composition of the acicular phase can be related once again to an averaging between the existing phases, Mg and 2Mg–Cu. Both the bright and dark phases mentioned earlier are discernible. The dark phase is a Mg supersaturated solid solution while the bright particles are non-dissolved Y.

As stated earlier, an XRD spectrum typical of an amorphous material was obtained only in the case of the melt spun specimen. However, the electron selected area diffraction patterns (SADP) given in Fig. 7*b*, with its rings being composed of many sharp spots instead of broad diffraction halos, shows evidence of the material being crystalline. Clear evidence for the crystallinity of the material is obtained from the high-resolution image (Fig. 8) in which different grains are discernible while the different orientations of adjacent grains can be clearly observed. Keeping in mind that the FFTs performed on a few grains (Fig. 8) simulate the electron diffraction process, one can treat it as additional evidence of the crystallinity of the material.

It is well known that when the XRD peaks become very broad the structural interpretation of the peak widths becomes ambiguous. It is difficult, however, to determine whether this broadening arises from the presence of very small, randomly oriented fragments of bulk crystal or from the existence of an amorphous structure. One example of this issue given in the literature[16] related to 75Pd–25Si. In its case the average crystal size is of the order of 2 nm. Spaepen[18] established a criterion for discriminating between the two cases; namely, the existence of either very fine grained materials or amorphous materials, determined by DSC. As stated by Spaepen,[18] the exothermic transformation of truly amorphous materials is qualitatively different from that of crystalline ones. In the former case, new crystals nucleate and grow, and the heat given off is the difference in enthalpy between the amorphous and the crystalline phases. A crystalline material, in contrast, simply undergoes grain growth and the heat given off during grain growth corresponds to the reduction in interfacial energy. The isothermal calorimetric signal for the grain growth process, according to Spaepen,[18] is a monotonically decreasing signal, which is qualitatively different from the peak observed when nucleation and growth take place.

However, no DSC analysis was conducted in the current study because transmission electron microscopy supplied sufficient evidence for the crystallinity of the material. Keeping in mind that even in a crystalline material the grain boundary is amorphous, by definition it may be claimed that obtaining an amorphous pattern involves the contribution of the grain boundaries. A rough estimation of the volume fraction of the grain boundaries can be obtained by applying simple geometry. Assuming that the grains are spherical with an average grain size of about 30 nm (not far from reality, as can be seen in Fig. 6) and that the width of the grain boundary region is about 1 nm (2–3 times the magnesium lattice parameter), it turns out that the volume fraction of the grain boundaries is about 19%. Furthermore, assuming that the width of the grain boundary region is about 5 nm (10–15 times the magnesium lattice parameter), it turns out that, for the same grain size, the volume fraction of the grain boundaries is about 70%. It seems that this contribution should not be neglected and that the amorphous XRD pattern obtained in the case of the melt spun specimen originates from both the contribution of the grain boundaries and the presence of very fine crystals. However, crystallinity of this microstructure was noted. It should not be ignored that the same morphology,

Published by Maney Publishing (c) IOM Communications Ltd

namely spherical grains having an average size of about 30 nm, was detected by HRSEM inside one of the dark particles of the permanent mould casting (Fig. 5). The mould was held in this case at −195°C, which means, in turn, that the cooling rate obtained was the highest among the permanent mould castings. It might be that this cooling rate refers to the beginning of the appearance of a fine structure obtained by the melt spinning process. However, understanding the kinetics of these phase transformations requires further research work.

Conclusions

- The microstructure of 80Mg–15Cu–5Y castings, obtained under five different cooling rates, was investigated and characterised by means of XRD, SEM and TEM and EDS analyses. An XRD spectrum typical for a completely amorphous material was recorded only in the case of the melt spinning process.
- In all cases of crystalline material, most of the structure consists of an acicular or a feather-like structure, and, concomitantly, the higher the cooling rate, the finer the structure. The phases identified were Mg and 2Mg–Cu while Y was detected both as non-dissolved particles and in a supersaturated Mg solid solution.
- TEM study and SADP revealed a crystalline structure even in the case of melt spinning. This finding was supported by high-resolution TEM. High-resolution SEM images revealed that the structure consists of fine spheres, each a few tens of nanometres in size.
- Difficulties in determining whether the XRD peak broadening arises from the presence of very small crystals or from the existence of an amorphous structure are well known and reported in the literature. Nevertheless, the average crystal size in the present study is relatively large.
- Further research work is still required in order to determine whether the amorphous behaviour is due to the contribution of the grain boundaries or the existence of the fine crystalline structure.

Acknowledgment

The authors wish to thank Dr. Y. Kauffmann for his assistance with the TEM study; thanks are also due to Mr. S. Avraham for TEM specimen preparation.

References

1. J. W. Hong, H. S. Kang, W. Y. Yoon and S. M. Lee: *Mater. Sci. Eng. A,* 2007, **449–451**, 727–732.
2. N. Schlorke, B. Weiss, J. Eckert and L. Schultz: *Nanostruct. Mater.,* 1999, **12**, 127–130.
3. S. Puech, J. J. Blandin and J. L. Soubeyoux: *Adv. Eng. Mater.*, 2007, **9**, 764–768.
4. D. Kim, B. J. Lee and N. J. Kim: *Scripta Mater.*, 2005, **52**, 969–972.
5. N. Pryds, M. Eldrup and A. Schrøder Pedersen: Proc. of the 22nd Risø International Symposium on Materials Science: 'Science of Metastable and Nanocrystalline Alloys Structure, Properties and Modeling', Risø National Laboratory, Roskilde, Denmark 2001, 377–382.
6. M. Savyak, S. Hirnyj, H.-D. Bauer, M. Uhlemann, J. Eckert, L. Schultz and A. Gebert: *J. Alloys Comp.*, 2004, **364**, 229–237.
7. M. Satta, M. Palumbo, P. Rizzi and M. Baricco: *Adv. Eng. Mater.*, 2007, **9**, 475–479.
8. A. Inoue and T. Masumoto: *Mater. Sci. Eng. A,* 1993, **173**, 1–8.
9. A. Inoue, T. Nakamura, N. Nishiyama and T. Masumoto: *Mater. Trans. JIM,* 1992, **10**, 937–945.
10. A. Inoue, A. Kato, T. Zhang, S. G. Kim and T. Masumoto: *Mater. Trans. JIM,* 1991, **32**, 609–616.
11. U. Wolff, N. Pryds and J. A. Wert: *Scripta Mater.*, 2004, **50**, 1385–1388.
12. G. Chen and M. Ferry: *J. Mater. Sci.*, 2007, **42**, 646–651.
13. S. G. Kim, A. Inoue and T. Masumoto: *Mater. Trans. JIM,* 1990, **31**, 929–934.
14. B. S. Murty and K. Hono: *Mater. Trans. JIM,* 2000, **41**, 1538–1544.
15. H. Ma, Q. Zheng, J. Xu, Y. Li and E. Ma: *J. Mater. Res.,* 2005, **20**, 2252–2255.
16. J. R. Davis and P. Allen, 'ASM Handbook', 10th edn; 1990, ASM, USA.
17. T. D. Massalski, 'Binary alloy phase diagrams', 2nd printing; 1987, ASM, USA.
18. F. Spaepen: *Mater. Res. Soc. Symp.*, 1989, **132**, 127–135.

Published by Maney Publishing (c) IOM Communications Ltd